PHYSICAL REVIEW C **95**, 041602(R) (2017)

Long-time drift of the isospin degree of freedom in heavy ion collisions

Yan Zhang (张嫣),[1] Junlong Tian (田俊龙),[2,*] Wenjing Cheng (程文静),[1] Fenhai Guan (关分海),[1] Yan Huang (黄彦),[1] Hongjie Li (李红洁),[1] Liming Lü (吕黎明),[1] Rensheng Wang (王仁生),[1,†] Yijie Wang (王轶杰),[1] Qianghua Wu (吴强华),[1] Han Yi (易晗),[1] Zhao Zhang (张钊),[1] Yixuan Zhao (赵亦轩),[1] Limin Duan (段利敏),[3] Rongjiang Hu (胡荣江),[3] Meirong Huang (黄美容),[3,‡] Genming Jin (靳根明),[3] Shilun Jin (金仕纶),[3] Chengui Lu (鲁辰桂),[3] Junbing Ma (马军兵),[3] Peng Ma (马朋),[3] Jiansong Wang (王建松),[3] Herun Yang (杨贺润),[3] Yanyun Yang (杨彦云),[3] Junwei Zhang (张俊伟),[3] Yapeng Zhang (张亚鹏),[3] Yingxun Zhang (张英逊),[4] Chunwang Ma (马春旺),[5] Chunyuan Qiao (乔春源),[2,5] Manyee Betty Tsang (曾敏儿),[6] and Zhigang Xiao (肖志刚)[1,§]

[1]*Department of Physics and Collaborative Innovation Center of Quantum Matter, Tsinghua University, Beijing 100084, China*
[2]*School of Physics and Electrical Engineering, Anyang Normal University, Anyang 455000, China*
[3]*Institute of Modern Physics, Chinese Academy of Sciences, Lanzhou 730000, China*
[4]*China Institute of Atomic Energy, Beijing 102413, China*
[5]*Institute of Particle and Nuclear Physics, Henan Normal University, Xinxiang 453007, China*
[6]*National Superconducting Cyclotron Laboratory, Michigan State University, East Lansing, Michigan 48864, USA*

(Received 7 October 2016; revised manuscript received 16 February 2017; published 24 April 2017)

The drift of the isospin degree of freedom (IDOF) is experimentally visualized through the wide-range angular distribution and the beam energy dependence of the isospin composition of light charged particles (LCP) produced in heavy ion collisions. It is evidenced that the net isospin transport is presented in the whole process from early dynamic emission to the statistical evaporation lasting to very late stage. Due to the long-time accumulation of the isospin effect, the angular distribution of the relative neutron excess summing over the LCPs is utilized as a sensitive probe to the symmetry energy. With S fixed at 28.3 MeV, a soft density dependence with $L = 33$–61 MeV (0.95 confidential level) at ρ_0 is circumstantially deduced using an improved quantum molecular dynamics transport model attached with a statistical emission afterburner.

DOI: 10.1103/PhysRevC.95.041602

The process of relaxation of a physical degree of freedom (DOF) is a matter of fundamental interest in all transport processes in nature. One such process occurs during the collision of two heavy ions at Fermi energies, in which the transport process is characterized by the relaxation of various DOFs including isospin [1], i.e., the evolution of the difference in the number of neutrons and protons. The transport of the isospin DOF (IDOF) in heavy ion collisions (HIC) manifests itself in the isospin fractionation, an analog phenomenon to the chemical distillation, which states that the neutrons are easier to be repelled to the gas phase due to the presence of the density-dependent symmetry energy $E_{\mathrm{sym}}(\rho)$ [2,3]. But it is not clear how fast the transport of IDOF is, given that no consistent conclusion on the equilibration of IDOF in HIC has been achieved so far. Early studies suggest the equilibration of IDOF is established [4–7]. However, nonequilibration has been demonstrated by increasing the beam energy so that the relaxation time constant of IDOF becomes longer than the thermal dynamic one [8–11]. Using the kinetic energy of quasiprojectiles as a clock [12], it has been shown the equilibration of IDOF is not as fast as the separation of the incident partners at peripheral collisions [13–15]. Clearly, these conclusions are obtained under varying conditions associated with the isospin diffusion, which refers to the transport of IDOF between the regions separated by the N/Z gradient. On the other hand, the isospin drift refers to the transport of IDOF driven by the density gradient. The later effect can be further viewed in well-designed experiments. For instance, it is shown that the transport of IDOF persists beyond 1200 fm/c and isospin drift takes effect [16–18]. As far as the isospin drift is concerned, a fundamental question is naturally raised about how fast the IDOF reaches equilibration and whether it is associated with a certain process.

Isospin drift and isospin diffusion are both related to $E_{\mathrm{sym}}(\rho)$ proportional to the chemical potential difference between proton and neutron in nuclear system. The density dependence of $E_{\mathrm{sym}}(\rho)$ influences not only the thermodynamic properties [19–22] and the collective motion [23] of finite hot nuclei, but also the structural properties of neutron stars [24–26] and the boundary of the nuclear chart [27,28]. However, it has been the most uncertain part of the equation of state (EOS) of neutron-rich nucleon matter so far [29]. Since the early attempt to extract $E_{\mathrm{sym}}(\rho)$ in the isospin diffusion experiments [30–32], progress on constraining $E_{\mathrm{sym}}(\rho)$ has been reported using various observables in HIC [33–42] with the value S and the slope L of $E_{\mathrm{sym}}(\rho)$ at ρ_0 being confined as $S = 32 \pm 2$ MeV and $L = 50 \pm 25$ MeV [43]. There is still room to reduce the uncertainty particularly of the slope L; while many studies aim currently for reliable estimations of the systematic error bars of the different probes, the search for more stringent probes is ongoing. A

*tjl@aynu.edu.cn
†Present address: School of Radiation Medicine and Protection, Soochow University, Suzhou 215123, China.
‡Present address: College of Physics and Electronics information, Inner Mongolia University for Nationalities, Tongliao, 028000, China.
§xiaozg@tsinghua.edu.cn

recent measurement characterizing the N/Z relaxation in subzeptosecond resolution suggests that the time dependence of the N/Z equilibration carries more information about the nuclear EOS [44]. Quantitative elucidation of $E_{\rm sym}(\rho)$ becomes one of the major motivations for rare isotope beam facilities [45,46]. For a recent review, we refer to Ref. [47].

Concerning the constraint of $E_{\rm sym}(\rho)$, the isospin drift at work has two physical consequences which are less discussed: (i) the low-density neck formed in HIC is more neutron rich and carries a wealth of information on $E_{\rm sym}(\rho)$ [48–52] and (ii) the softness of $E_{\rm sym}(\rho)$ has significant influence on the liquid-gas transition of nuclear matter [53–59], since the two phases can be distinguished in density. Hence, novel isospin observables related to the long-time isospin drift process [18] at work in liquid-gas transition [20,60] offer opportunities to further constrain $E_{\rm sym}(\rho)$ at $\rho < \rho_0$.

Our particular interest on isospin drift has a twofold motivation: (i) to visualize the long-time feature of isospin drift and (ii) to identify a sensitive probe of $E_{\rm sym}(\rho)$ related to isospin drift because the persisting accumulation of the work of isovector force enhances the sensitivity of the observable on $E_{\rm sym}(\rho)$. We focus on the analysis of light charged particles (LCPs) since they carry highly sensitive information of $E_{\rm sym}(\rho)$ [51,61].

In this paper, we present the experimental results on the angular distribution of the isotopic yield ratio of the LCPs in Ar+Au at 30 MeV/u. Based on the collision kinetics, the angular distribution of the neutron richness of LCPs is translated into the long-time transport of IDOF ranging from early dynamic emission of the overlapped region to the statistical evaporation of the hot target-like fragments (TLF) lasting to late stage. Careful comparison to the simulations using an improved quantum molecular dynamics (ImQMD) model coupled to the GEMINI afterburner has been conducted to constrain $E_{\rm sym}(\rho)$ with high sensitivity.

The experiment was performed on the Radioactive Ion Beam Line at Lanzhou (RIBLL). The beam of 30 MeV/u ^{40}Ar was delivered by the Heavy Ion Research Facility at Lanzhou to bombard the 1-μm-thick Au target installed in the scattering chamber at the end of RIBLL. Four parallel plate avalanche counters (PPAC) with sensitive area of $30 \times 35\,\mathrm{cm}^2$ were installed to measure the coincident fission fragments. The center of each PPAC was located in the same horizontal plane with the beam line and the PPAC-target distance was 35 cm. The polar angles of the four PPACs were $\pm 30^\circ$ and $\pm 60^\circ$, respectively. The PPACs were running with 6-mbar isobutane at 490 V so that the LCP and intermediate mass fragments were suppressed. To measure the LCPs in coincidence with fission fragments, nine telescopes, each consisting of two Si(Au) ΔE units backed with one CsI crystal of 3 cm thickness for E measurement, were installed from 19° to 160° in the laboratory. The distance to target $l_{\rm d}$, the polar angle in laboratory $\theta_{\rm lab}$, the azimuthal angle ϕ, the collimator diameter $d_{\rm c}$, and the thicknesses of ΔE_1 and ΔE_2 units are listed in Table I. In this Rapid Communication, we present the inclusive data of the LCPs measured by the telescopes.

Figures 1(a) and 1(c) present the distribution of the inclusive isotopic yield ratio $R_{\rm I}$ for $Z = 1$ and $Z = 2$ LCPs as a function of $\theta_{\rm lab}$. It is shown that the neutron-deficient isotopic ratios, $Y(p)/Y(d)$ or $Y(^3\mathrm{He})/Y(\alpha)$, increase with $\theta_{\rm lab}$, while for the neutron-rich isotopic ratios $Y(t)/Y(d)$ or $Y(^6\mathrm{He})/Y(\alpha)$, a decreasing trend is observed. It suggests that the LCPs emitted at small angles are relatively more neutron rich.

TABLE I. The parameters of the 9 LCP telescopes.

Telescope no.	$l_{\rm d}$ (mm)	$\theta_{\rm lab}$ (deg)	ϕ (deg)	$d_{\rm c}$ (mm)	ΔE_1 (μm)	ΔE_2 (μm)
1	301	37	69	8.0	150.0	200.0
2	231	19	39	8.0	75.0	200.0
3	231	19	141	8.0	75.0	200.0
4	556	45	170	8.0	50.0	200.0
5	304	74	39	12.0	30.0	200.0
6	236	70	13	5.0	50.0	300.0
7	230	161	37	5.5	25.0	300.0
8	266	109	196	12.0	30.0	200.0
9	590	135	110	5.0	50.0	300.0

The angular behavior of the isotopic ratio can be interpreted in terms of the time evolution of IDOF from early dynamic emission to the later statistic emission. Due to the kinematics of the fixed target experiment, the emissions at intermediately small angles are contributed more by the dynamic emission of short time scale, while the emissions at large angles are mainly contributed by the statistical emission of the compound nuclei. This scenario can be schematically illustrated by a simplified moving-source analysis to α spectra at various angles. Here we assume the LCPs are mainly contributed by two sources: One is the intermediate velocity source (IVS) with higher source velocity and higher temperature, and the other is the compound nuclei source (CNS) with lower source velocity and lower temperature. Figure 2(a) displays the best-fit curves superimposed on the spectra at 74°, 70°, and 37°. The fitting technique is similar with that in Ref. [62]. The Coulomb barrier $B_{\rm C}$ and the temperature T of CNS are obtained by a single-source fit to the spectra

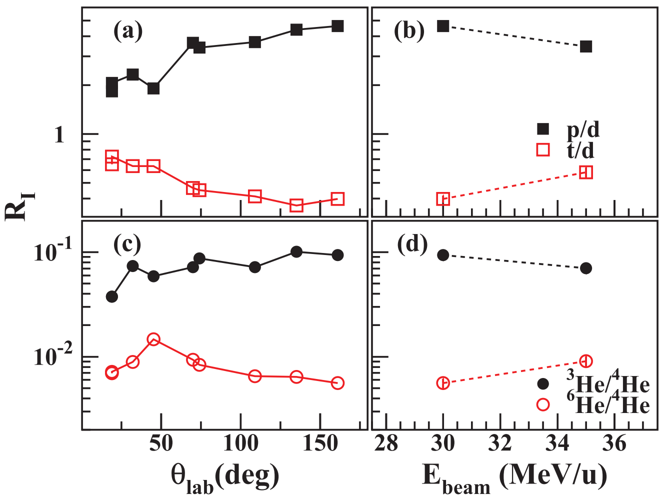

FIG. 1. The inclusive isotopic ratio for $Z = 1$ (upper) and $Z = 2$ (lower) isotopes as a function of laboratory angle at 30 MeV/u (left) and of beam energy (right).

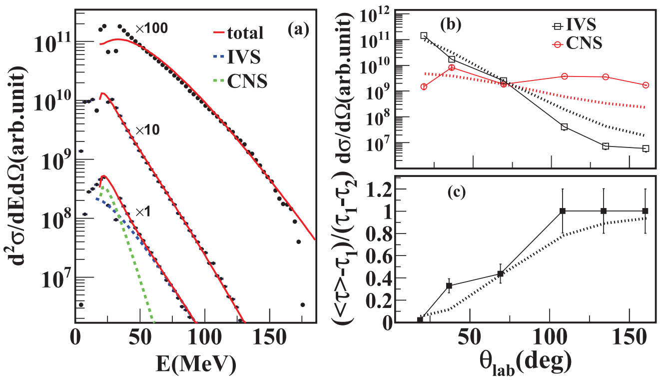

FIG. 2. (a) The energy spectra of α particles fitted by two moving sources. (b) LCP yield as a function of θ_{lab} for the emissions from IVS (black square) and CNS (open circle), respectively; see text. (c) The average emission time $(\langle\tau\rangle - \tau_1)$ seen by the LCPs as a function of θ_{lab} in units of $(\tau_2 - \tau_1)$.

at 135° and 161°. Then the IVS parameters are optimized by fitting the spectrum at 19° with two moving sources. By applying the parameters to fit all spectra with the multiplicity being a free parameter at each angle, the intensities of the two sources can be obtained. The optimized Coulomb barrier, source velocity, and the temperature parameters are listed in Table II. Figure 2(b) presents the LCP yield as a function of θ_{lab} for IVS and CNS emission, respectively. The reference dotted curves represent the calculations, assuming all moving source parameters are fixed as obtained at 70°. It is shown that the multiplicity decreases with θ_{lab} more rapidly for IVS than CNS emission, in accordance with the results of intermediate mass fragments observed in the same reaction [63]. The different forward-angle concentration between CNS and IVS is expected due to the different source velocities. Adjusting the relative contribution of the two sources by varying θ_{lab}, one can readily probe different emission stage on average, since the emission time scale is very different for these two sources. The time scale τ_1 of the IVS is deduced at about 10^2 fm/c using the small angle correlation technique [64,65] and using the temperature evolution in HIC [66]. For the statistical emission of the CNS, the typical emission time scale τ_2 is on the order of 10^3 fm/c. In the simplified two-source picture, the average time scale of the particle emission, expressed as $\langle\tau\rangle = (n_1\tau_1 + n_2\tau_2)/(n_1 + n_2)$ where n_1 and n_2 denote the α yield from IVS and CNS, respectively, shows a continuous increasing trend with θ_{lab} as shown in Fig. 2(c), where the quantity $(\langle\tau\rangle - \tau_1)/(\tau_2 - \tau_1) = n_2/(n_1 + n_2)$ is plotted. In such a way the ordinate is independent of the values of τ_1 and τ_2.

In a more realistic view of the collision, it is reasonable to assume that the mean time of LCP emission is shorter on average at smaller angles, although it is less straightforward to draw a quantitative relationship between θ_{lab} and $\langle\tau\rangle$. In this regard, the isotopic ratio varying with θ_{lab} shown in Fig. 1(a) evidences that the LCPs emitted earlier are more neutron rich and the neutron concentration keeps decreasing until a very late stage of the vaporization of the hot target-like fragment (TLF). It confirms the isospin-dependent hierarchy of particle emission derived by analyzing the energy spectra of $Z = 1$ species in Ar+Au at 35 MeV/u [62].

It is worthwhile to note that the correspondence between $\langle\tau\rangle$ and θ_{lab} is smeared, if not vanished, in the target rapidity region, because the contributions are dominated by the statistical emission of the TLF with a time scale much longer than the dynamic emission. To visualize the time evolution of the LCP's isospin composition over the long statistical decay chain, it is important to measure the beam energy dependence of the average N/Z of the LCPs at large angles. Data at $E_{\mathrm{beam}} = 30$ and 35 MeV/u are collected here. The later is taken from our earlier experiment [62]. Figures 1(b) and 1(d) compare the isotopic yield ratios at 160° for the two beam energies. It is shown that for the emissions at $E_{\mathrm{beam}} = 35$ MeV/u where the TLFs are at higher excitation energy, the relative yields of neutron-rich (neutron-poor) isotopes like t and ^{6}He (p and ^{3}He) are higher (lower) than those at 30 MeV/u. It suggests that the nuclear vapor sampled by the LCPs is more neutron rich if the liquid drop is hotter.

Isospin drift and isospin diffusion are usually entangled with respective contributions depending on specific process in HIC. The analysis focuses on the LCPs representing the vapor distinguished from the heavy nuclei by density. Considering the process, either early in dynamic emission or late in evaporation, that the LCPs are drawn from the interior of the hot nuclei and emitted at surface with the path passing through different density regions, we suggest that isospin drift is the main mechanism governing the dynamics of IDOF here.

The continuous decrease of the neutron richness with θ_{lab} and with lowering E_{beam} at large angles has an important implication. The net isospin transport is presented in the whole procedure from early dynamic emission to the statistical evaporation lasting to a very late stage, showing the distinguishing feature from the fast equilibration in isospin diffusion process widely discussed.

Next, we quantify the influence of $E_{\mathrm{sym}}(\rho)$ by defining an angular observable, expecting the sensitivity is enhanced due to the lasting accumulation of isospin effect in the long-time process. An ImQMD model [67,68] is applied to simulate the reactions until 1000 fm/c, then a statistical evaporation model GEMINI is appended to simulate the decay of the hot nuclei. In the model, each nucleon is represented by a coherent state of a Gaussian wave packet [69]. The nucleonic potential energy U_{loc} is obtained from the integration of the Skyrme energy density functional $V_{\mathrm{loc}}[\rho(\mathbf{r})]$,

$$V_{\mathrm{loc}} = \frac{\alpha}{2}\frac{\rho^2}{\rho_0} + \frac{\beta}{\sigma+1}\frac{\rho^{\sigma+1}}{\rho_0^{\sigma}} + \frac{g_0}{2\rho_0}(\nabla\rho)^2 + \frac{C_s}{2}\left[\frac{\rho^{\gamma+1}}{\rho_0^{\gamma}} - \frac{\kappa_s}{\rho_0}(\nabla\rho)^2\right]\delta^2 + g_\tau\frac{\rho^{\eta+1}}{\rho_0^{\eta}}, \quad (1)$$

TABLE II. The source velocity v_s, Coulomb barrier B_C, and temperature T of CNS and IVS.

Source	v_s (cm/ns)	B_C (MeV)	T (MeV)
CNS	0.9	18.6	5.2
IVS	3.7	3.5	9.5

where $\delta = (\rho_n - \rho_p)/(\rho_n + \rho_p)$ is the isospin asymmetry. The first three terms are obtained from the potential energy functional of Skyrme forces directly, and the last term is from the kinetic energy density functional using the Thomas-Fermi approximation. The fourth term is the symmetry potential including both the bulk and the surface terms. C_s is the strength parameter, and γ gives the density dependence of symmetry potential. The different density dependence of $E_{\rm sym}(\rho)$ can be realized by varying γ value. In this work, we adopt the parameter set IQ3 [70,71] with $\alpha = 207$ MeV, $\beta = 138$ MeV, and $\sigma = 7/6$, $g_0 = 18$ MeVfm^2, $C_s = 32$ MeV, $\kappa_s = 0.08$ fm^2, $g_\tau = 14$ MeV, and $\eta = 5/3$. At the end of the ImQMD calculations, clusters are recognized by a minimum spanning tree (MST) algorithm [69]. The excitation energy of each cluster is input into GEMINI code to simulate the statistic decay. Detailed description of GEMINI can be found in Refs. [72,73].

It is known that the yield of nucleons (light clusters) is usually overestimated (underestimated) in QMD type of transport models due to the intrinsic weakness of the clustering. The clustering deficiency calls for an alternative observable to constrain $E_{\rm sym}(\rho)$, instead of using the absolute values of the LCP yield ratios. Since the angular dependence of the isotopic composition reflects the time evolution of the isospin transport and the stiffness of $E_{\rm sym}(\rho)$ determines how fast the neutrons are repelled to the gas, the decreasing rate of the relative neutron richness of the LCPs can be used to probe $E_{\rm sym}(\rho)$ without knowing necessarily the details of the time evolution of IDOF. Here, in order to circumvent the problem that very high yield of the $N = Z$ species blurs the variation of $\langle N/Z\rangle$ when counting an individual element, we investigate the total neutron excess normalized to the coalescence invariant proton yield by

$$\frac{Y_{\rm n,ex}}{Y_{\rm p,CI}} = \frac{\sum y_i(N_i - Z_i)}{\sum y_i Z_i}, \tag{2}$$

where y_i, N_i, and Z_i are the yield and the numbers of n and p of the species i summing over the $Z = 1$ and 2 LCPs, respectively.

Figure 3 presents the ratio $Y_{\rm n,ex}/Y_{\rm p,CI}$ as a function of $\theta_{\rm lab}$. The crosses denote the data while the curves are the

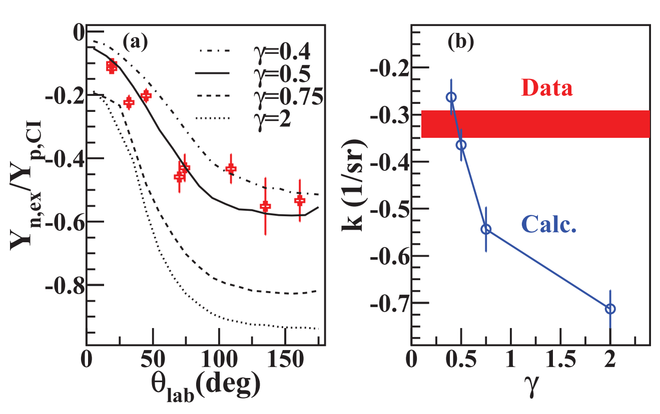

FIG. 3. (a) Angular distribution of the relative neutron richness (symbols) summed over the LCPs in comparison with the ImQMD+GEMINI simulations (curves) using $\gamma = 0.4$, 0.5, 0.75, and 2, respectively. (b) The slope k of the linear fit to the data (filled band, 1σ width) below 90° compared with simulations (open circles).

ImQMD+GEMINI simulations. The trend that the ratio $Y_{\rm n,ex}/Y_{\rm p,CI}$ decreases rapidly below 90° and exhibits a flat tendency at large angles is well reproduced. However, due to the clustering deficiency in transport model, the curves from the simulation show offset depending on γ in the whole angular range. Despite the ordinate offset assumed to be the same in the whole angular range, one notices that the decreasing rate of the $Y_{\rm n,ex}/Y_{\rm p,CI}$ differentiates the stiffness of $E_{\rm sym}(\rho)$. It decreases more rapidly with $\theta_{\rm lab}$when the $E_{\rm sym}(\rho)$ becomes stiffer. Translating the angular behavior to time evolution, it means qualitatively that a stiffer $E_{\rm sym}(\rho)$ results in a faster isospin fractionation driving the neutrons to the vapor. This is consistent with previous transport model calculations [74], where the secondary decay with GEMINI was turned off. It supports the qualitative scenario that a change of the density dependence of $E_{\rm sym}(\rho)$ modifies the neutron richness of the emission source as input of GEMINI, which in turn leads to a difference in the isotopic yields. Quantitatively, a linear fit has been conducted to the data points between 19° and 90° with

$$\frac{Y_{\rm n,ex}}{Y_{\rm p,CI}} = k\theta_{\rm lab} + b, \tag{3}$$

where the slope k describes the average decreasing rate of $Y_{\rm n,ex}/Y_{\rm p,CI}$ with $\theta_{\rm lab}$ for $Z = 1$ and 2 species. As shown in Fig. 3 (b), k depends very sensitively on γ. Clearly a soft $E_{\rm sym}(\rho)$ with γ situating between 0.4 and 0.5 is circumstantially favored by the data.

The uncertainty of this single measurement has been estimated in the current model framework. In the energy region of the present studies, it has been shown that the parameters of the MST coalescence procedure has insignificant influence on the isospin observables. For instance, it is less than 8% to the single n/p ratio as the first-order isospin observable [75]. Since the Pauli blocking is important here, the contribution of the two-body collisions is also limited and influences slightly the isotopic ratios (<1%) [76]. If the IQMD calculation is extended to 3000 fm/c and the GEMINI burner is turned off, both the value of $Y_{\rm n,ex}/Y_{\rm p,CI}$ and the slope on $\theta_{\rm lab}$ are consistent with the calculations with $\gamma = 0.4$–0.5, although the ratios are increasingly enhanced at small angles with γ approaching to 2. Thus, an uncertainty of 10% is empirically assigned to the ratios $Y_{\rm n,ex}/Y_{\rm p,CI}$ for the model calculations. With this uncertainty level, the calculated points of $Y_{\rm n,ex}/Y_{\rm p,CI}$ vs $\theta_{\rm lab}$ in the same angular range are fitted and the uncertainties of k are plotted by the error bars in Fig. 3(b). The uncertainty of the experimental ratios $Y_{\rm n,ex}/Y_{\rm p,CI}$ includes the contributions from both the statistical fluctuation and 5% (10%) systematic uncertainties arising from the detection threshold effect and the particle identification cuts for $Z = 1$ (2) isotopes. As a result of the regression analysis, the expected value of γ is derived as $\gamma = 0.46$ with the standard deviation $s_\gamma = 0.025$. The slope of the symmetry energy at saturation density of $L = 33$–61 MeV is then deduced at 0.95 confidential level with $n_{\rm DOF} = 1$ and S being fixed at 28.3 MeV. This range of L is consistent with the latest update of $L = 20$–66 MeV by analyzing the electric dipole polarizability of various nuclei [77,78], with $L = 52.7 \pm 22.5$ MeV from the global optical potential analysis [79] and $L = 51.8 \pm 7.2$ MeV from the proton radioactivity analysis [80].

We would like to caution here that further comparisons are still needed between the data and different model calculations using simultaneous multiobservables before accurate and convincing $E_{\mathrm{sym}}(\rho)$ can be achieved, because intertwined links between the model parameters may exist and some physics are differently treated or even missing in existing models. As one can see, important discussions have been raised on the convolution of other effects in the extraction of $E_{\mathrm{sym}}(\rho)$, including effective n-p mass splitting [81], short-range correlations [82–86], tensor forces [87], and parameter correlations [88]. It is suggested that a robust constraint of $E_{\mathrm{sym}}(\rho)$ relies on the analysis in the multidimensional parameter space using a valid model. The new probe introduced in this work provides a new line to crosscheck the description of HIC in transport models [89] and adds a new observable in the covariant analysis to pin down the systematic uncertainties of $E_{\mathrm{sym}}(\rho)$ parametrizations in transport calculations. Further experiments utilizing 4π detector or including neutron measurement over wide angular range are important. For the latter, the coalescence invariant n/p ratio can be adopted in place of Eq. (2) to overcome the weakness of transport model on clustering.

In summary, it is reported that the neutron richness of the LCPs decreases with the emitting angle in laboratory over a wide range and with lowering the beam energy at large angles in the Ar+Au reaction. It suggests that the isospin drift, which refers to the transport of IDOF from the high-density region (liquid phase) to the low-density region (vapor phase), occurs from early dynamic emission to statistical evaporation at very late stage. The slow feature of isospin drift is different from the fast relaxation of the IDOF in isospin diffusion.

Due to the accumulation of the effect of $E_{\mathrm{sym}}(\rho)$ in the long-time isospin drift process, the angular distribution of the relative neutron excess of the LCPs representing the gas phase is proved to be a sensitive probe to the symmetry energy. By analyzing the decreasing rate of the relative neutron excess of the LCPs with angle, a soft $E_{\mathrm{sym}}(\rho)$ with $L = 33$–61 MeV is circumstantially deduced at 0.95 confidential level fixing $S = 28.3$ MeV.

This work is supported by the National Science Foundation of China under Grants No. 11375094, No. U1332207, and No. 11475004 and by Tsinghua University Initiative Scientific Research Program. J.L.T. has been supported by the Domestic Visiting Scholarship Program of the Ministry of Education, China, under Grant No. 2015609043 during his stay in THU. We acknowledge the detector group from IMP, CAS for providing the CsI crystals and the machine staff for delivering the beam.

[1] Y. Iwata, T. Otsuka, J. A. Maruhn, and N. Itagaki, Phys. Rev. Lett. **104**, 252501 (2010).
[2] H. S. Xu, M. B. Tsang, T. X. Liu, X. D. Liu, W. G. Lynch, W. P. Tan, A. Vander Molen, G. Verde, A. Wagner, H. F. Xi *et al.*, Phys. Rev. Lett. **85**, 716 (2000).
[3] S. Hudan, R. Alfaro, B. Davin, Y. Larochelle, H. Xu, l. Beaulieu, T. Lefort, R. Yanez, R. T. de Souza, R. J. Charity *et al.*, Phys. Rev. C **71**, 054604 (2005).
[4] B. Gatty, D. Guerreau, M. Lefort, X. Tarrago, J. Galin, B. Cauvin, J. Girard, and H. Nifenecker, Nucl. Phys. A **253**, 511 (1975).
[5] T. H. Chiang, D. Guerreau, P. Auger, J. Galin, B. Gatty, X. Tarrago, and J. Girard, Phys. Rev. C **20**, 1408 (1979).
[6] O. V. Lozhkin and W. Trautmann, Phys. Rev. C **46**, 1996 (1992).
[7] G. Ademard *et al.* (INDRA Collaboration), Eur. Phys. J. A **50**, 33 (2014).
[8] B. A. Li and C. M. Ko, Phys. Rev. C **57**, 2065 (1998).
[9] S. J. Yennello *et al.*, Phys. Lett. B **321**, 15 (1994).
[10] L.-W. Chen, L. Ge, X. Zhang, and F. Zhang, J. Phys. G **23**, 211 (1997).
[11] Z. Y. Sun *et al.*, Phys. Rev. C **82**, 051603(R) (2010).
[12] A. Olimi, in *Nuclear Collisions from the Mean-Field into the Fragmentation Regime*, edited by C. Detraz and P. Kienle (Elsevier, Amsterdam, 1991), p. 71.
[13] H.-Y. Wu *et al.*, Phys. Lett. B **538**, 39 (2002).
[14] G. A. Souliotis, P. N. Fountas, M. Veselsky, S. Galanopoulos, Z. Kohley, A. McIntosh, S. J. Yennello, and A. Bonasera, Phys. Rev. C **90**, 064612 (2014).
[15] G. A. Souliotis, M. Veselsky, and S. J. Yennello, Phys. Lett. B **588**, 35 (2004).
[16] S. Hudan, A. B. McIntosh, R. T. de Souza, S. Bianchin, J. Black, A. Chbihi, M. Famiano, M. O. Frégeau, J. Gauthier, D. Mercier *et al.*, Phys. Rev. C **86**, 021603(R) (2012).
[17] K. Brown, S. Hudan, R. T. de Souza, J. Gauthier, R. Roy, D. V. Shetty, G. A. Souliotis, and S. J. Yennello, Phys. Rev. C **87**, 061601 (2013).
[18] S. Hudan and R. T. deSouza, Eur. Phys. J. A **50**, 36 (2014).
[19] A. B. McIntosh, A. Bonasera, Z. Kohley, P. J. Cammarata, K. Hagel, L. Heilborn, J. Mabiala, L. W. May, P. Marini, A. Raphelt *et al.*, Phys. Rev. C **87**, 034617 (2013).
[20] A. B. McIntosh *et al.*, Eur. Phys. J. A **50**, 35 (2014).
[21] Z. G. Xiao *et al.*, Phys. Lett. B **639**, 436 (2006).
[22] L. W. Chen, V. Greco, C. M. Ko, and B. A. Li, Phys. Rev. Lett. **90**, 162701 (2003).
[23] G. Colo, U. Garg, and H. Sagawa, Eur. Phys. J. A **50**, 26 (2014).
[24] J. M. Lattimer and M. Prakash, Science **304**, 536 (2004).
[25] A. W. Steiner, M. Prakash, J. M. Lattimer, and P. J. Ellis, Phys. Rept. **411**, 325 (2005).
[26] C. J. Horowitz *et al.*, J. Phys. G **41**, 093001 (2014).
[27] R. Wang and L. W. Chen, Phys. Rev. C **92**, 031303 (2015).
[28] K. Oyamatsu, K. Iida, and H. Koura, Phys. Rev. C **82**, 027301 (2010).
[29] B. A. Li, L. W. Chen, and C. M. Ko, Phys. Rept. **464**, 113 (2008).
[30] M. B. Tsang, T. X. Liu, L. Shi, P. Danielewicz, C. K. Gelbke, X. D. Liu, W. G. Lynch, W. P. Tan, G. Verde, A. Wagner *et al.*, Phys. Rev. Lett. **92**, 062701 (2004).

[31] B. A. Li, C. B. Das, S. Das Gupta, and C. Gale, Nucl. Phys. A **735**, 563 (2004).
[32] L. W. Chen, C. M. Ko, and B. A. Li, Phys. Rev. Lett. **94**, 032701 (2005).
[33] M. A. Famiano, T. Liu, W. G. Lynch, M. Mocko, A. M. Rogers, M. B. Tsang, M. S. Wallace, R. J. Charity, S. Komarov, D. G. Sarantites *et al.*, Phys. Rev. Lett. **97**, 052701 (2006).
[34] T. Li *et al.*, Phys. Rev. Lett. **99**, 162503 (2007).
[35] G. Cardella, G. Giuliani, I. Lombardo, M. Papa, L. Acosta, C. Agodi, F. Amorini, A. Anzalone, L. Auditore, I. Berceanu *et al.*, Phys. Rev. C **85**, 064609 (2012).
[36] M. B. Tsang, Y. Zhang, P. Danielewicz, M. Famiano, Z. Li, W. G. Lynch, and A. W. Steiner, Phys. Rev. Lett. **102**, 122701 (2009).
[37] M. Liu, N. Wang, Z. X. Li, and F. S. Zhang, Phys. Rev. C **82**, 064306 (2010).
[38] Z. Kohley, L. W. May, S. Wuenschel, A. Bonasera, K. Hagel, R. Tripathi, R. Wada, G. A. Souliotis, D. V. Shetty, S. Galanopoulos *et al.*, Phys. Rev. C **82**, 064601 (2010).
[39] Z. Kohley, G. Christian, T. Baumann, P. A. DeYoung, J. E. Finck, N. Frank, M. Jones, J. K. Smith, J. Snyder, A. Spyrou, and M. Thoennessen, Phys. Rev. C **88**, 041601(R) (2013).
[40] J. B. Natowitz, G. Röpke, S. Typel, D. Blaschke, A. Bonasera, K. Hagel, T. Klähn, S. Kowalski, L. Qin, S. Shlomo, R. Wada, and H. H. Wolter, Phys. Rev. Lett. **104**, 202501 (2010).
[41] S. Kowalski, J. B. Natowitz, S. Shlomo, R. Wada, K. Hagel, J. Wang, T. Materna, Z. Chen, Y. G. Ma, L. Qin *et al.*, Phys. Rev. C **75**, 014601 (2007).
[42] L. Ou, Z. Xiao, H. Yi, N. Wang, M. Liu, and J. Tian, Phys. Rev. Lett. **115**, 212501 (2015).
[43] M. B. Tsang, J. R. Stone, F. Camera, P. Danielewicz, S. Gandolfi, K. Hebeler, C. J. Horowitz, J. Lee, W. G. Lynch, Z. Kohley *et al.*, Phys. Rev. C **86**, 015803 (2012).
[44] A. Jedele, A. B. McIntosh, K. Hagel, M. Huang, L. Heilborn, Z. Kohley, L. W. May, E. McCleskey, M. Youngs, A. Zarrella, and S. J. Yennello, Phys. Rev. Lett. **118**, 062501 (2017).
[45] B. Hong *et al.*, Eur. Phys. J. A **50**, 49 (2014).
[46] L. Lü, H. Yi, Z. Xiao, M. Shao, S. Zhang, G. Xiao, and N. Xu, Sci. China Phys. Mech. Astron. **60**, 012021 (2017).
[47] B. A. Li, A. Ramos, G. Verde, and I. Vidana, Eur. Phys. J. A **50**, 9 (2014).
[48] E. De Filippo and A. Pagano, Eur. Phys. J. A **50**, 32 (2014).
[49] E. De Filippo *et al.*, Phys. Rev. C **86**, 014610 (2012).
[50] V. Baran, M. Colonna, M. Di Toro, M. Zielinska-Pfabe, and H. H. Wolter, Phys. Rev. C **72**, 064620 (2005).
[51] Z. Q. Feng, Phys. Rev. C **94**, 014609 (2016).
[52] Y. Zhang, C. Zhou, J. Chen, N. Wang, K. Zhao, and Z. Li, Sci. China Phys. Mech. Astron. **58**, 112002 (2015).
[53] J. B. Elliott *et al.* (ISiS Collaboration), Phys. Rev. Lett. **88**, 042701 (2002).
[54] L. G. Moretto, J. B. Elliott, and L. Phair, Phys. Rev. C **72**, 064605 (2005).
[55] L. G. Moretto, K. A. Bugaev, J. B. Elliott, R. Ghetti, J. Helgesson, and L. Phair, Phys. Rev. Lett. **94**, 202701 (2005).
[56] J. Pochodzalla *et al.*, Phys. Rev. Lett. **75**, 1040 (1995).
[57] P. Chomaz, M. Colonna, and J. Randrup, Phys. Rept. **389**, 263 (2004).
[58] P. Chomaz and F. Gulminelli, Phys. Lett. B **447**, 221 (1999).
[59] B. K. Sharma and S. Pal, Phys. Rev. C **81**, 064304 (2010).
[60] B. A. Li, L. W. Chen, H. R. Ma, J. Xu, and G. C. Yong, Phys. Rev. C **76**, 051601 (2007).
[61] M. Kaur, S. Gautam, and R. K. Puri, Nucl. Phys. A **955**, 133 (2016).
[62] R. S. Wang, Y. Zhang, Z. G. Xiao, J. L. Tian, Y. X. Zhang, Q. H. Wu, L. M. Duan, G. M. Jin, R. J. Hu, S. F. Wang *et al.*, Phys. Rev. C **89**, 064613 (2014).
[63] U. Milkau *et al.*, Phys. Rev. C **44**, R1242(R) (1991).
[64] E. Bauge, A. Elmaani, R. A. Lacey, J. Lauret, N. N. Ajitanand, D. Craig, M. Cronqvist, E. Gualtieri, S. Hannuschke, T. Li *et al.*, Phys. Rev. Lett. **70**, 3705 (1993).
[65] Z. Y. He *et al.*, Phys. Rev. C **57**, 1824 (1998).
[66] J. Wang *et al.* (NIMROD Collaboration), Phys. Rev. C **72**, 024603 (2005).
[67] N. Wang, Z. Li, and X. Wu, Phys. Rev. C **65**, 064608 (2002).
[68] N. Wang, Z. Li, X. Wu, J. l. Tian, Y. X. Zhang, and M. Liu, Phys. Rev. C **69**, 034608 (2004).
[69] J. Aichelin, Phys. Rept. **202**, 233 (1991).
[70] V. Zanganeh, N. Wang, and O. N. Ghodsi, Phys. Rev. C **85**, 034601 (2012).
[71] C. Li, J. Tian, L. Ou, and N. Wang, Phys. Rev. C **87**, 064615 (2013).
[72] R. J. Charity *et al.*, Nucl. Phys. A **483**, 371 (1988).
[73] R. J. Charity, L. G. Sobotka, J. Cibor, K. Hagel, M. Murray, J. B. Natowitz, R. Wada, Y. El Masri, D. Fabris, G. Nebbia *et al.*, Phys. Rev. C **63**, 024611 (2001).
[74] Q. Wu, Y. Zhang, Z. Xiao, R. Wang, Y. Zhang, Z. Li, N. Wang, and R. H. Showalter, Phys. Rev. C **91**, 014617 (2015).
[75] Y. Zhang, Z. Li, C. Zhou, and M. B. Tsang, Phys. Rev. C **85**, 051602 (2012).
[76] Y. Zhang, D. D. S. Coupland, P. Danielewicz, Z. Li, H. Liu, F. Lu, W. G. Lynch, and M. B. Tsang, Phys. Rev. C **85**, 024602 (2012).
[77] X. Roca-Maza, X. Viñas, M. Centelles, B. K. Agrawal, G. Colò, N. Paar, J. Piekarewicz, and D. Vretenar, Phys. Rev. C **92**, 064304 (2015).
[78] Z. Zhang and L. W. Chen, Phys. Rev. C **90**, 064317 (2014).
[79] C. Xu, B. A. Li, and L. W. Chen, Phys. Rev. C **82**, 054607 (2010).
[80] N. Wan, C. Xu, and Z. Ren, Phys. Rev. C **94**, 044322 (2016).
[81] B. A. Li and L. W. Chen, Mod. Phys. Lett. A **30**, 1530010 (2015).
[82] B. J. Cai and B. A. Li, Phys. Rev. C **92**, 011601 (2015).
[83] O. Hen, B. A. Li, W. J. Guo, L. B. Weinstein, and E. Piasetzky, Phys. Rev. C **91**, 025803 (2015).
[84] O. Hen *et al.*, Science **346**, 614 (2014).
[85] B. J. Cai and B. A. Li, Phys. Rev. C **93**, 014619 (2016).
[86] B. A. Li, W. J. Guo, and Z. Shi, Phys. Rev. C **91**, 044601 (2015).
[87] C. Xu and B. A. Li, Phys. Rev. C **81**, 064612 (2010).
[88] Y. Zhang, M. B. Tsang, and Z. Li, Phys. Lett. B **749**, 262 (2015).
[89] J. Xu *et al.*, Phys. Rev. C **93**, 044609 (2016).